GFZ
Helmholtz-Zentrum
für Geoforschung

Originally published as:

Zhong, Y., Picotti, V. (2025): Accelerated Tectonic Activity, Rather Than Paleolake Regression, Drives Increased Pleistocene River Incision Along the Jinshan Gorge in the Middle Yellow River. - Tectonics, 44, 5, e2024TC008501.

https://doi.org/10.1029/2024TC008501

Institutional Repository GFZpublic: https://gfzpublic.gfz-potsdam.de/

HELMHOLTZ
SPITZENFORSCHUNG FÜR
GROSSE HERAUSFORDERUNGEN

Check for updates

Tectonics®

RESEARCH ARTICLE
10.1029/2024TC008501

Key Points:

- Paleolake regression at the outlet of the Jinshan Gorge could only generate a short-lived upstream-migrating incision-rate pulse
- Integration with a paleolake upstream of the Jinshan Gorge would generate greatest increase in incision rate at the gorge's upstream end
- Increased Pleistocene incision rates along the gorge are likely due to enhanced tectonic activity on the fault bounding the southern gorge

Supporting Information:

Supporting Information may be found in the online version of this article.

Correspondence to:

Y. Zhong,
yuezhi.zhong@gfz.de

Citation:

Zhong, Y., & Picotti, V. (2025). Accelerated tectonic activity, rather than paleolake regression, drives increased Pleistocene river incision along the Jinshan Gorge in the middle Yellow River. *Tectonics*, *44*, e2024TC008501. https://doi.org/10.1029/2024TC008501

Received 3 JUL 2024
Accepted 14 APR 2025

Author Contributions:

Conceptualization: Yuezhi Zhong, Vincenzo Picotti
Data curation: Yuezhi Zhong
Formal analysis: Yuezhi Zhong, Vincenzo Picotti
Funding acquisition: Yuezhi Zhong
Investigation: Yuezhi Zhong
Methodology: Yuezhi Zhong, Vincenzo Picotti
Supervision: Vincenzo Picotti
Validation: Vincenzo Picotti
Visualization: Yuezhi Zhong
Writing – original draft: Yuezhi Zhong
Writing – review & editing: Yuezhi Zhong, Vincenzo Picotti

© 2025. American Geophysical Union. All Rights Reserved.

Accelerated Tectonic Activity, Rather Than Paleolake Regression, Drives Increased Pleistocene River Incision Along the Jinshan Gorge in the Middle Yellow River

Yuezhi Zhong[1,2] **and Vincenzo Picotti**[1]

[1]Department of Earth Sciences, ETH Zurich, Zurich, Switzerland, [2]GFZ German Research Centre for Geosciences, Potsdam, Germany

Abstract The Jinshan Gorge in the middle Yellow River, northern China, currently connecting the upstream Hetao Graben to the downstream Weihe Graben, is hypothesized to have recently developed, which implies changing incision rates along the gorge. However, different integration processes have been proposed, such as paleolake regression in the Weihe Graben or integration with a paleolake in the Hetao Graben. These different mechanisms imply different timings, from the Late Miocene to the Late Pleistocene. In this study, we model variations in channel profiles and incision in response to different integration processes using the stream power law. We show that variations due to paleolake regression in the Weihe Graben or integration with paleolake in the Hetao Graben are inconsistent with the incision history preserved by river terraces and reconstructed by inverse analysis of tributary profiles. Instead, a recent increase in the slip rate of the Weihe Graben's boundary faults can explain the main features. Inverse analysis of channel profiles along the Jinshan Gorge suggests that relative uplift rates were a steady ∼0.04 mm/yr before the Early Pliocene, and increased to ∼0.16 mm/yr at present, especially since the Middle-Late Pleistocene. Our analysis is supported by further data from paleoseismic, drilling and paleostress studies.

Plain Language Summary Recently, numerous studies have been undertaken along the Jinshan Gorge, trying to relate its incision history with the integration of the Yellow River. However, most of these studies take deposit records at some sites to represent the history of the entire, more than 700 km long gorge, and several distinct hypotheses have been proposed. To test these hypotheses, we model the evolution of the gorge's channel profile (a curve of elevation against distance along stream), and compare results to the present-day profile. We find that simulated profiles corresponding to existing hypotheses for the integration of the Jinshan Gorge were inconsistent with incision history recorded by river terraces and channel profiles, so that such integration is unlikely to have occurred. Instead, our results indicate that Pleistocene incision rate variations are dominated by accelerated motion of the fault bounding the southern gorge. This interpretation aligns with observations from drill cores, paleoseismic studies, and stress regime data. We thus conclude that tectonics, not lake drainage, shaped the gorge.

1. Introduction

The Yellow River, China, originates on the Northeast Tibetan Plateau, and follows a circuitous path, initially flowing north, then east and south, nearly encircling the Ordos Block, before flowing east to the North China Plain and discharging into the Bohai Sea (Figure 1a). How the Yellow River, especially its middle reach surrounding the Ordos Block, developed this drainage pattern is debated (Liang et al., 2015; Lin et al., 2001; Zheng et al., 2007). When the current drainage pattern was established is also highly controversial, with proposed timings ranging from the Late Miocene to the Late Pleistocene (Craddock et al., 2010; Kong et al., 2014; Liang et al., 2015; Lin et al., 2001; Y. Liu, 2020; Pan et al., 2011, 2012; Perrineau et al., 2011; Xiao et al., 2020; Zheng et al., 2007). Some studies have suggested that the Yellow River evolved by connecting various basins along its course by river capture and headward erosion (Craddock et al., 2010; Jiang et al., 2007; Ke, 2012; Liang et al., 2015). Of these basins, the Hetao Graben and the Weihe Graben are separated by the greatest distance (∼700 km), so the development of the Jinshan Gorge connecting them was a critical step in the integration of the Yellow River and the establishment of its present planform (Figures 1b and 1c).

Three different integration processes have been proposed for the establishment of the middle Yellow River (Hu et al., 2017; Jiang et al., 2007; Liang et al., 2015; Lin et al., 2001; Pan et al., 2012). The first hypothesis is that

10.1029/2024TC008501

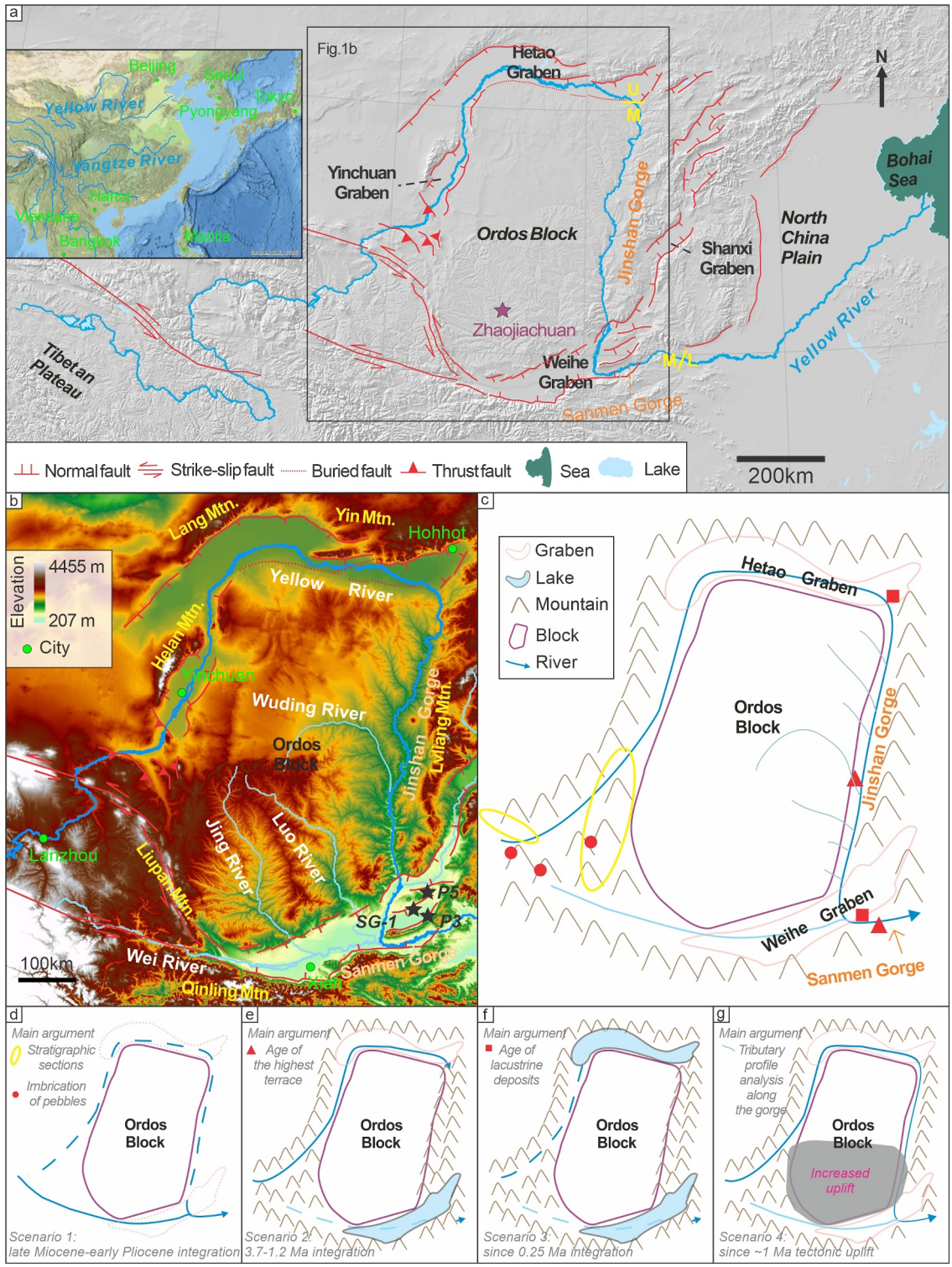

Figure 1. Topography, channels and sketches for settings currently and before hypothetical integration in the middle Yellow River. (a) The blue lines show the main channel of the Yellow River, which is divided into upper (U), middle (M) and lower (L) reaches. The red lines show major fault structures around the Ordos Block. (b) Topography in the middle Yellow River. Trunk channel shown in dark blue and main tributaries shown in light blue. Locations of borehole shown in black star. (c) Current setting in the middle Yellow River. The Jinshan Gorge forms a present-day connection between the Hetao Graben in the north and the Weihe Graben in the south. Locations of field evidences to support each hypothesis below are also shown. (d) Proposed setting before integration in Late Miocene-Early Pliocene by Lin et al. (2001). (e) Proposed setting before integration between 3.7 and 1.2 Ma by Pan et al. (2012). (f) Proposed setting before integration around 0.25 Ma by Liang et al. (2015). (g) Proposed setting and driving factor by Zhong et al. (2022).

19449194, 2025, 5, Downloaded from https://agupubs.onlinelibrary.wiley.com/doi/10.1029/2024TC008501 by Helmholtz-Zentrum Potsdam GFZ, Wiley Online Library on [19/06/2025]. See the Terms and Conditions (https://onlinelibrary.wiley.com/terms-and-conditions) on Wiley Online Library for rules of use; OA articles are governed by the applicable Creative Commons License

19449194, 2025, 5, Downloaded from https://agupubs.onlinelibrary.wiley.com/doi/10.1029/2024TC008501 by Helmholtz-Zentrum Potsdam GFZ, Wiley Online Library on [19/06/2025]. See the Terms and Conditions (https://onlinelibrary.wiley.com/terms-and-conditions) on Wiley Online Library for rules of use; OA articles are governed by the applicable Creative Commons License

channels currently looping around the Ordos Block only developed in the Late Miocene-Early Pliocene in response to the collision of India into Eurasia and rifting around the Ordos Block (Lin et al., 2001). Before that time, the Yellow River flowed directly from its exit from the Tibetan Plateau across the Weihe Graben and discharged to the lower reach, following the path of the present-day Wei River, now a tributary (Figure 1d, scenario 1). The second hypothesis is that the Jinshan Gorge and the Sanmen Gorge were entrenched between 3.7 and 1.2 Ma (Hu et al., 2017; Pan et al., 2012). The Yellow River is proposed to have been blocked by the Sanmen Horst (located in the Sanmen Gorge), forming an endorheic paleolake in the Weihe Graben (Hu et al., 2017) (Figure 1e, scenario 2). Finally, the third hypothesis is that paleolakes existed both in the Hetao Graben and the Weihe Graben, and due to the entrenchment of the Sanmen Gorge at ∼0.25 Ma the paleolake in the Weihe Graben regressed (Jiang et al., 2007; Liang et al., 2015, 2022). This regression is proposed to have induced base level fall, forming a knickpoint at the outlet of the Jinshan Gorge that has by now retreated ∼275 km upstream. Connection between the gorge and the paleolake in the Hetao Graben occurred at ∼0.1 Ma, representing the final integration of the Yellow River (Liang et al., 2015) (Figure 1f, scenario 3).

Some studies also suggest that no integration took place in the middle Yellow River during the Pleistocene (J. Xiong et al., 2024; Zhong et al., 2022, 2024). Combined with detrital zircon dating of Neogene-Quaternary sediments and topographic investigation along the Jinshan Gorge, J. Xiong et al. (2024) suggest that the middle Yellow River was already integrated in the Late or even the Early Miocene. Based on an analysis of tributary channel profiles and terraces along the Jinshan Gorge, they propose that the southern gorge has experienced increased incision rates since the Pleistocene, whereas the northern gorge maintained steady incision rates through that time (Zhong et al., 2022, 2024). To explain the incision rate variations, Zhong et al. (2022) suggested that the southern gorge was uplifted by sub-lithospheric processes, such as deep mantle flow (Figure 1g, scenario 4).

In this paper, we explore the ultimate cause of incision rate variations along the Jinshan Gorge of the Yellow River: whether they are due to river integration, associated with increased upstream drainage area or sudden base-level fall, or due to tectonic processes, such as uplift of the southern gorge as proposed by Zhong et al. (2022). We first model channel profile development and associate incision variations for scenarios 2–4 (scenario 1 is not simulated since its integration time and process have not been precisely defined). We then compare results with the observed trunk profile and incision history recorded by river terraces and inferred by inverse modeling from the channel profiles of tributaries along the Jinshan Gorge (Zhong et al., 2022, 2024) (Figure 2). We further model the response to accelerated uplift with or without spatial variation and to temporal climate change along the Jinshan Gorge. Our results provide the basis for a river inversion analysis along the Jinshan Gorge to infer the relative uplift history. Finally, we interpret our results in the context of additional records of climate change, in particular drill cores, paleoseismic studies and stress regime observations.

2. Regional Background

In this section we describe the geologic setting of the Ordos Block and the incision history of the Yellow River along the Jinshan Gorge since the Late Miocene as inferred from river terraces and from tributary channel profile analysis. The geologic setting mainly includes the tectonic evolution and geology surrounding the block, the extents of grabens upstream and downstream of the Jinshan Gorge, and relevant fault activities, which are closely related to scenarios to be tested and parameter values in our model simulations. The reconstructed incision history along the Jinshan Gorge is described as we will also use it to test different scenarios.

2.1. Geologic Settings

During the Mesozoic, mountains such as the Qinling and Yin around the Ordos Block uplifted rapidly in response to Indo-China and Yanshan orogenesis (Figure 1b) (Y. Zhang & Liao, 2006). Between these mountain ranges, a large retro-belt intermontane basin developed with thousands of meters of terrigenous clastic sediments, forming the present-day Ordos Block (Clinkscales et al., 2021; Ritts et al., 2009). In the middle-late Jurassic, and finally after the early Cretaceous, the Ordos basin was inverted (Y. Zhang & Liao, 2006), resulting in considerable erosion. As a result of Indo-Asian and Pacific-Asian collision and subduction and associated changes in tectonic stresses around the Ordos Block, an extensional regime reactivated the former basin boundaries, resulting in formation of grabens since the late Cenozoic (Shi et al., 2020; Tapponnier & Molnar, 1976; Y. Zhang et al., 1998).

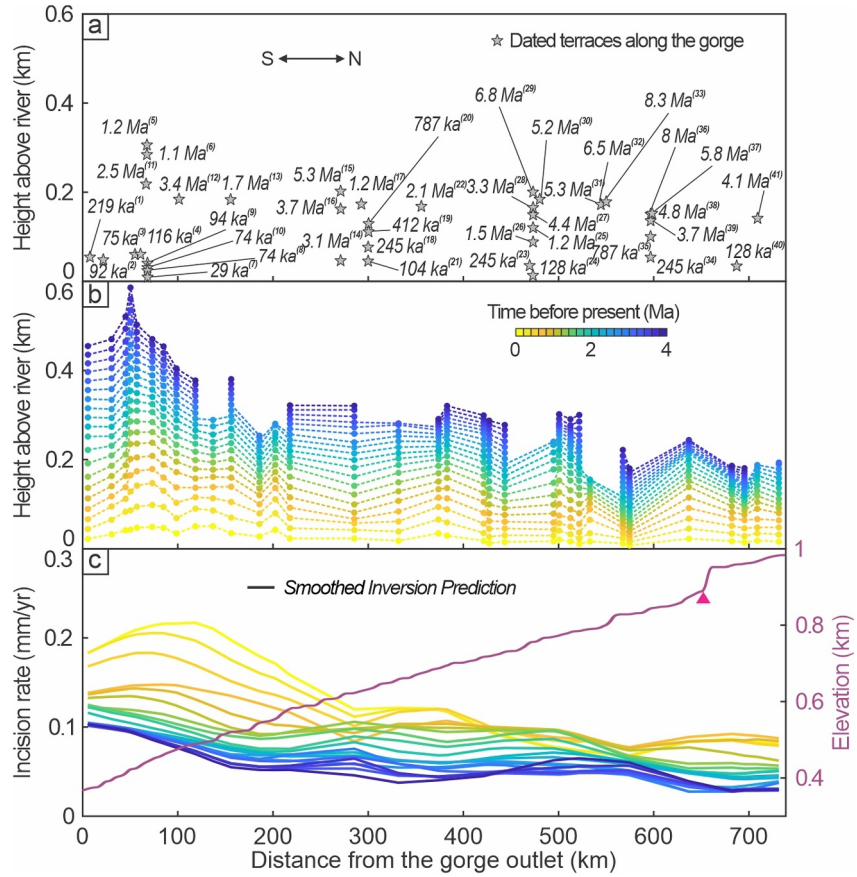

Figure 2. Dated river terraces, incision variations reconstructed from an inversion analysis of tributary profiles. (a) Dated river terraces along the Jinshan Gorge (Table S1 in Supporting Information S1). (b) Incision variations reconstructed from an inversion analysis. Absolute time scaling obtained with $K = 1.03 \times 10^{-5}$ $m^{0.3}$/yr. (c) Continuous curves give spatially smoothed estimated incision rates using a smoothing window of 100 km. Purple curve shows modern gorge longitudinal profile. Red triangle marks the ~70 m high Wanjiazhai Dam at around 650 km upstream. Absolute rate and time obtained with $K = 1.03 \times 10^{-5}$ $m^{0.3}$/yr. The figure is modified from Zhong et al. (2022).

The bedrock of the present-day Ordos Block comprises a generally uniform stratigraphy of siliciclastic rocks (Ritts et al., 2009).

The W-E trending Hetao Graben at the upstream end of the Jinshan Gorge is ~440 km long and ~80 km wide (Figures 1a and 1b). An array of normal faults cut the northeastern margin of the graben, and some buried faults are distributed across the graben's southern margin as well as within it (China Earthquake Administration, 1988). Cenozoic strata, with a thickness of over 5 km, are well developed within the Hetao Graben, mostly to the west, with the lower part characterized by reddish-brown, purplish red or gray lacustrine clay and the upper part characterized by gray-black clay interbedded with brown clay (China Earthquake Administration, 1988). Quaternary sediments vary in thickness from 0 to 2.5 km, mainly composed of thick gray or green-greyish mudstone and yellow sandstone, thought to represent a sedimentary environment of alternating fluvio-lacustrine and desert conditions (China Earthquake Administration, 1988; B. Li et al., 2017).

The development of the Weihe Graben (Figures 1a and 1b), at the downstream end of the Jinshan Gorge, began at ~50 Ma, as constrained by apatite fission track thermochronology (J. Liu et al., 2013). Subsidence rates peaked at ~10 Ma, which might be linked with the northeastward growth of the Tibetan Plateau (J. Liu et al., 2013). Cenozoic strata within the graben have a thickness of over 7 km (Y. Zhang et al., 1998). Faults in the graben are characterized by normal-slip motion, and have been active with an average rate of ~2–3 mm/yr during the Late Pleistocene-Holocene (Rao et al., 2014, 2017).

19449194, 2025, 5, Downloaded from https://agupubs.onlinelibrary.wiley.com/doi/10.1029/2024TC008501 by Helmholtz-Zentrum Potsdam GFZ, Wiley Online Library on [19/06/2025]. See the Terms and Conditions (https://onlinelibrary.wiley.com/terms-and-conditions) on Wiley Online Library for rules of use; OA articles are governed by the applicable Creative Commons License

19449194, 2025, 5, Downloaded from https://agupubs.onlinelibrary.wiley.com/doi/10.1029/2024TC008501 by Helmholtz-Zentrum Potsdam GFZ, Wiley Online Library on [19/06/2025]. See the Terms and Conditions (https://onlinelibrary.wiley.com/terms-and-conditions) on Wiley Online Library for rules of use; OA articles are governed by the applicable Creative Commons License

There is a distinct difference in tectonic activity between the Ordos Block and its peripheral grabens. The Ordos Block is thought to have been tectonically stable since the Mesozoic with very limited shortening in rare fold and thrust belts and little seismicity (Chen et al., 2009; Y. Li et al., 2014). To the contrary, the peripheral grabens show intense tectonic activity with active rifting and frequent earthquakes (Y. Li et al., 2014; Rao et al., 2014).

2.2. Incision History Inferred From River Terraces

Terrace surfaces have been identified and dated along much of the trunk stream in the Jinshan Gorge, with clusters of ages emerging at ~5 Ma, ~4 Ma, ~1.2 Ma, ~245 ka and ~100 ka (Figure 2a, Table S1 in Supporting Information S1). Some important features can be identified. At ~70 km upstream from the gorge outlet the strath height of a ~1.2 Ma terrace is ~200 m higher than the strath terrace at ~480 km upstream from the gorge outlet with a similar estimated age of ~1.24 Ma (Cao, 2012; Hu et al., 2016) (Figure 2a). Similarly, the difference in heights of strath terraces with ages of ~100 ka in the south and the north is 35 ± 15 m (Cao, 2012; Guo et al., 2012; Liang, 2017). In addition, several studies based on river terrace correlation along the gorge suggest that terraces broadly diverge in the downstream direction (S. Cheng et al., 2002; Hu et al., 2016; Liang et al., 2015), which indicates increased river incision rates toward the south. However, the sparse temporal distribution of trunk stream terrace ages precludes a thorough interpretation of the middle Yellow River's integration history on the basis this record alone.

2.3. Incision History Reconstructed From Tributary Channel Profile Analysis

Incision variations have also been reconstructed from inverse analysis of channel profiles from tributaries that drain into the Jinshan Gorge (Zhong et al., 2022, 2024). The reconstructed incision history, which extends from 4 Ma to the present day, shows higher amounts of incision in the southern gorge and a long-term (over the past ~1 Ma) increase in incision rate (Figures 2b and 2c), which is consistent with the inferences from trunk stream river terraces (Section 2.2). In addition, an incision history with higher temporal resolution is reconstructed, which enables a more thorough interpretation of the integration history of the middle Yellow River.

3. Methods

3.1. Simulating Channel Profile Evolution Using the Stream Power Law

The evolution of a channel profile is usually modeled with the detachment-limited stream power model (Crosby & Whipple, 2006; Howard & Kerby, 1983; Whipple & Tucker, 1999), where transport capacity is assumed to exceed the imposed sediment load. In this model, river bed elevation at a point x along the channel changes by the difference between the rock uplift rate (or base level fall rate), $U(x,t)$, and the incision rate, $E(x,t)$:

$$\frac{dz(x,t)}{dt} = U(x,t) - E(x,t) \tag{1}$$

$E(x,t)$ is expressed as:

$$E(x,t) = KA(x,t)^m S(x,t)^n \tag{2}$$

where K is an erodibility coefficient, influenced by rock strength, bed roughness, precipitation rates and basin hydrology; A is upstream drainage area; S is channel gradient; and m and n are both positive constants.

We used a total model run time of 4 Ma, the same time span used in the existing reconstructed incision history (Section 2.3, Zhong et al., 2022, 2024). >70% of published river terraces ages from the Jinshan Gorge are within this range (Table S1 in Supporting Information S1). In testing the different scenarios described above (Figures 1d–1g), we imposed perturbations at either 0.1, 0.25, or 1.2 Ma, and modeled the channel profile development without or with spatial change in U, Z_{out}, A_{out}, and K (Table 1). Except for the scenario with temporally varying K, we set the initial U to 0.08 mm/yr and K to 1.03×10^{-5} $m^{0.3}$/yr following Zhong et al. (2024). This best-fit K value, which represents an average erodibility of the river over time, was obtained by optimizing the misfit between published terrace ages, with ages ranging from 0.03 to 8 Ma, and ages predicted from channel profile analysis (Zhong et al., 2024). We extracted A from a hydrologically conditioned version of the digital elevation model (DEM) (Lehner et al., 2008). We resampled the DEM to a resolution of 90 m, and

Tectonics
10.1029/2024TC008501

Table 1
Parameter Set Up for Each Scenario in Model Simulation

Scenario no.	Z_{out} [a] (m)	A_{out} [b] (10^3 km^2)	K (10^{-5} m$^{0.3}$/yr)	U changes in space?	U (mm/yr)
Scenario 2	515 when t [c] > 1.2 Ma 365 when $t \leq$ 1.2 Ma	119 when t > 1.2 Ma 509 when $t \leq$ 1.2 Ma	1.03 all time	No	0.08 all time
Scenario 3	515 when t > 0.25 Ma 365 when $t \leq$ 0.25 Ma	119 when t > 0.1 Ma 509 when $t \leq$ 0.1 Ma	1.03 all time	No	0.08 all time
Scenario 4	365 all time	509 all time	1.03 all time	Yes	Where D[d] > 100 km 0.08 all time Where $D \leq$ 100 km 0.08 when t > 1.2 Ma 0.2 when $t \leq$ 1.2 Ma
Scenario 5	365 all time	509 all time	1.03 all time	Yes	Where D > 500 km 0.08 all time Where $D \leq$ 500 km 0.08 when t > 1.2 Ma 0.2 when $t \leq$ 1.2 Ma
Scenario 6	365 all time	509 all time	1.03 all time	No	0.08 when t > 1.2 Ma 0.2 when $t \leq$ 1.2 Ma
Scenario 7.1 (Scenario 7.2)	365 all time	509 all time	1.03 all time	Yes	Where D > 100 (500) km 0.08 all time Where $D \leq$ 100 (500) km 0.08 when t > 1.2 Ma Linearly increase to 0.2 when $t \leq$ 1.2 Ma
Scenario 8.1 (Scenario 8.2)	365 all time	509 all time	1.03 all time	Yes	Where D > 100 (500) km 0.08 all time Where $D \leq$ 100 (500) km 0.08 when t > 1.2 Ma In-step increase to 0.2 when $t \leq$ 1.2 Ma
Scenario 9.1 (Scenario 9.2)	365 all time	509 when t > 1.2 Ma 16 (95) when $t \leq$ 1.2 Ma	1.03 all time	Yes	Where D > 100 (500) km 0.08 all time Where $D \leq$ 100 (500) km 0.08 when t > 1.2 Ma 0.2 when $t \leq$ 1.2 Ma
Scenario 10.1 (Scenario 10.2)	365 all time	509 when t > 1.2 Ma 16 (95) when $t \leq$ 1.2 Ma	1.03 all time	Yes	Where D > 100 (500) km 0.08 all time Where $D \leq$ 100 (500) km 0.08 when t > 1.2 Ma Linearly increase to 0.2 when $t \leq$ 1.2 Ma
Scenario 11.1 (Scenario 11.2)	365 all time	509 when t > 1.2 Ma 16 (95) when $t \leq$ 1.2 Ma	1.03 all time	Yes	Where D > 100 (500) km 0.08 all time Where $D \leq$ 100 (500) km 0.08 when t > 1.2 Ma In-step increase to 0.2 when $t \leq$ 1.2 Ma
Scenario 12.1 (Scenario 12.2) (Scenario 12.3)	365 all time	509 all time	1.03 all time	Yes	Where D > 757 (100) (500) km 0.08 all time Where $D \leq$ 757 (100) (500) km 0.08 when t > 1.2 Ma Linear reduction in U from the gorge outlet to upstream when $t \leq$ 1.2 Ma
Scenario 13	365 all time	509 all time	Vary with P[e] change	No	0.08 all time

[a]Elevation at the outlet. [b]Drainage area at the outlet. [c]Time. [d]Distance from the gorge outlet. [e]Precipitation.

19449194, 2025, 5, Downloaded from https://agupubs.onlinelibrary.wiley.com/doi/10.1029/2024TC008501 by Helmholtz-Zentrum Potsdam GFZ, Wiley Online Library on [19/06/2025]. See the Terms and Conditions (https://onlinelibrary.wiley.com/terms-and-conditions) on Wiley Online Library for rules of use; OA articles are governed by the applicable Creative Commons License

applied a smooth window of 1 km to obtain the value of A every kilometer along the Jinshan Gorge. We set m and n to 0.35 and 1, respectively. These values correspond to a m/n ratio of 0.35, which best minimizes the dispersion of χ-z plots of tributaries in the study area (Willett et al., 2014).

Here we ran four types of simulation with 12 scenarios in total (Table 1), mostly corresponding to integration processes proposed by previous studies and described above: type 1 included scenario 2, with perturbations in outlet elevation and drainage area occurring at 1.2 Ma; type 2 included scenario 3, with the same perturbations as type 2 but occurring at 0.25 Ma; type 3 included scenarios 4–12, with various perturbations in uplift rates in space and time; type 4 included scenario 13, with perturbations in K that vary with temporal climate changes. We explored type 3 with more scenarios for two reasons: (a), we find that simulated evolutions of channel profiles and associated incision rates driven by variations in uplift rates showed some features consistent with the incision history reconstructed from tributary terraces and channel profile analysis, which we will discuss in Section 5.1; (b), a lack of considerable spatial changes in uplift rate along the Jinshan Gorge is a prerequisite to obtain a reliable relative uplift history inferred from channel profile inversion analysis along the Jinshan Gorge.

An inflection in χ-z plots for the Jing and Luo Rivers, tributaries to the Yellow River, implies a base level fall of 150 ± 50 m (Zhong et al., 2022), if the inflection is a result of paleo-lake regression in the Weihe Graben. As such, for scenarios 2 and 3, we set Z_{out} to 515 m initially, and suddenly dropping to 365 m (the modern outlet elevation extracted from DEM) to simulate base level.

For scenarios with temporally enhanced uplift rate (scenarios 4–12), we set U to increase suddenly, linearly, and in-step from the initial value of 0.08 mm/yr to 0.2 mm/yr at 1.2 Ma, based approximately on estimated recent incision rates from tributary inversion analysis (Zhong et al., 2022, 2024).

Scenarios 2, 3 and 9–11 included a change in upstream drainage area. At present, the upstream drainage area at the inlet of the Jinshan Gorge is about 390×10^3 km^2, increasing by about 119×10^3 km^2 to about 509×10^3 km^2 at the gorge's outlet. In scenarios 2 and 3, the Hetao Graben is assumed to be disconnected from the Jinshan Gorge, with a drainage divide existing prior to 1.2 Ma (scenario 2) or 0.1 Ma (scenario 3). As such, we set the upstream drainage to 119×10^3 km^2 prior the connection and increasing to 509×10^3 km^2 afterward. In scenarios 9–11, we set initial A_{out} to 509×10^3 km^2 (i.e., the Hetao Graben and the Jinshan Gorge had already been connected). After enhanced uplift occurred since 1.2 Ma, a lake formed, inhibiting erosion and violating the assumption that stream power is proportional to upstream drainage area. To account for this effect, we decreased drainage area for zones of enhanced uplift.

For the scenario with temporal variations in K (scenario 13), we took changes in >19 μm grain-size fraction from the Zhaojiachuan loess section (Figure 1a) on the Ordos Block (An et al., 2001) to be inversely proportional to K through time (Figure S1 in Supporting Information S1), as the grain-size fraction (K) is negatively (positively) correlated with precipitation rates. We used average values of the >19 μm grain-size fraction for the past 4 Ma (31.74%) and of K (1.03×10^{-5} m$^{0.3}$/yr) as reference values to compute K from >19 μm grain-size fraction. We then resampled the inferred K values to a temporal resolution of 0.025 Ma (Figure S1c in Supporting Information S1).

3.2. Channel Profile Inversion Analysis

Changes in uplift relative to the base-level of a drainage basin will induce variations in incision of the drainage network. Variations in incision rate will introduce inflections to the network's profiles that propagate upstream from base level. In this way, the channel profiles record the history of relative uplift. With an inverse analysis of the channel profiles, this uplift history can be recovered. Inverse methods have been proposed to recover temporally varying, spatially uniform uplift histories (Goren et al., 2014; Roberts & White, 2010), as well as uplift histories that are functions of both space and time (Fox et al., 2014; Roberts et al., 2012).

Here, we apply a spatially uniform uplift model following Goren et al. (2014), with the assumption that all points along drainage networks share a common uplift history. In this case, the present elevation relative to base level at a point x along a channel can be expressed as:

19449194, 2025, 5, Downloaded from https://agupubs.onlinelibrary.wiley.com/doi/10.1029/2024TC008501 by Helmholtz-Zentrum Potsdam GFZ, Wiley Online Library on [19/06/2025]. See the Terms and Conditions (https://onlinelibrary.wiley.com/terms-and-conditions) on Wiley Online Library for rules of use; OA articles are governed by the applicable Creative Commons License

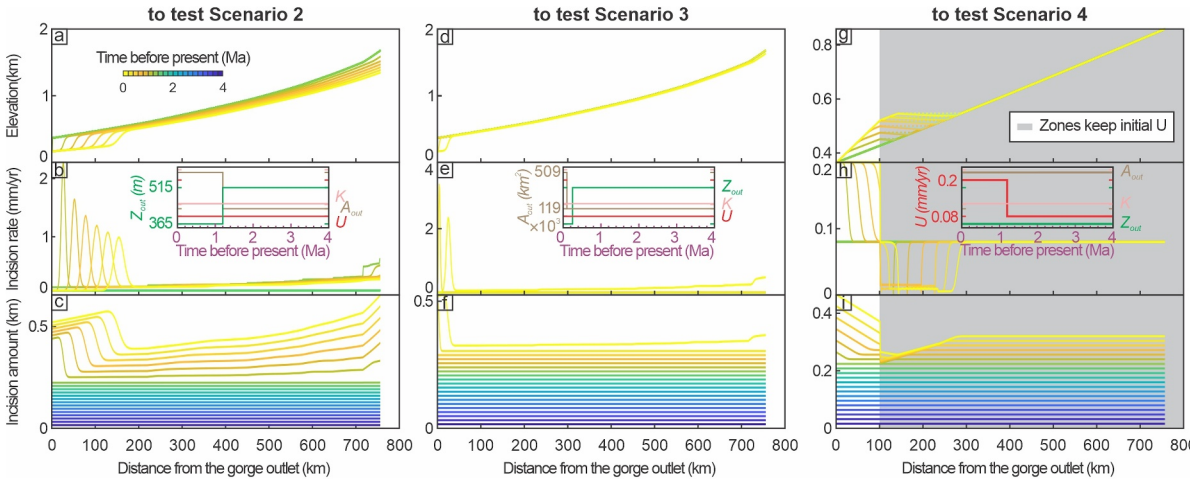

Figure 3. Changes in simulated channel profiles, incision rate and incision amount from 4 Ma to present with different perturbations. (a–c) Dropped outlet elevation from 515 to 365 m and added upstream drainage area of 390 * 10^3 km^2 at 1.2 Ma, and with constant uplift rate and K value from 4 Ma to present. (d–f) Dropped outlet elevation from 515 to 365 m at 0.25 Ma and added upstream drainage area of 390 * 10^3 km^2 at 0.1 Ma, and with constant uplift rate and K value from 4 Ma to present. (g–i) Suddenly increased relative uplift rate from 0.08 mm/yr to 0.2 mm/yr since 1.2 Ma, but the variations are only applied within 100 km upstream from the gorge outlet, and with constant upstream drainage area, outlet elevation and K from 4 Ma to present.

$$z(0,x) = \int_{-\tau(x)}^{0} U(t)\,dt \tag{3}$$

where $\tau(x)$ is the time taken for a perturbation to propagate upstream from base level to point x, defined as (Whipple & Tucker, 1999):

$$\tau(x) = \int_{0}^{x} \frac{dx}{KA(x)^m S(x)^{n-1}} \tag{4}$$

With a constraint on the value of K, $\tau(x)$ can be calculated, and Equation 3 can be solved. A regional estimate of K has been calculated using all published river terrace data along the Jinshan Gorge by (Zhong et al., 2024). The inversion processes have been described by Zhong et al. (2022). We will discuss in Sections 5.1 and 5.2 the implications of our assumption of spatially uniform uplift, given the large region traversed by the 700 km long gorge.

4. Results

4.1. Simulated Evolution With Perturbations in Outlet Elevation and Drainage Area Occurring at 1.2 Ma (Scenario 2)

We observe that base level fall at 1.2 Ma introduced a retreating inflection at the gorge outlet. Meanwhile, increased upstream drainage area caused a general reduction in slope, most visible downstream and upstream of the retreating inflection (Figure 3a). Near the gorge outlet a short-lived pulse in incision rate was generated (Figure 3b), but, after the inflection retreated away, incision rates returned to 0.08 mm/yr, equal to the background uplift rate. Further upstream, we find that incision rates increased as the inflection propagates passed, but the amplitude of the incision pulse decreased with distance from the gorge outlet (Figure 3b). We also observe that the total amount of incision was highest near the gorge outlet and at the upstream end of the gorge (Figure 3c), but the timing of incision varied: near the gorge outlet, where base level fall dominates, the timing of incision at a given point depended on when the inflection propagates passed that point; near the upstream end of the gorge, where the increase in drainage area dominates, the amount of incision increased steadily from 1.2 Ma (Figure 3c). We

19449194, 2025, 5, Downloaded from https://agupubs.onlinelibrary.wiley.com/doi/10.1029/2024TC008501 by Helmholtz-Zentrum Potsdam GFZ, Wiley Online Library on [19/06/2025]. See the Terms and Conditions (https://onlinelibrary.wiley.com/terms-and-conditions) on Wiley Online Library for rules of use; OA articles are governed by the applicable Creative Commons License

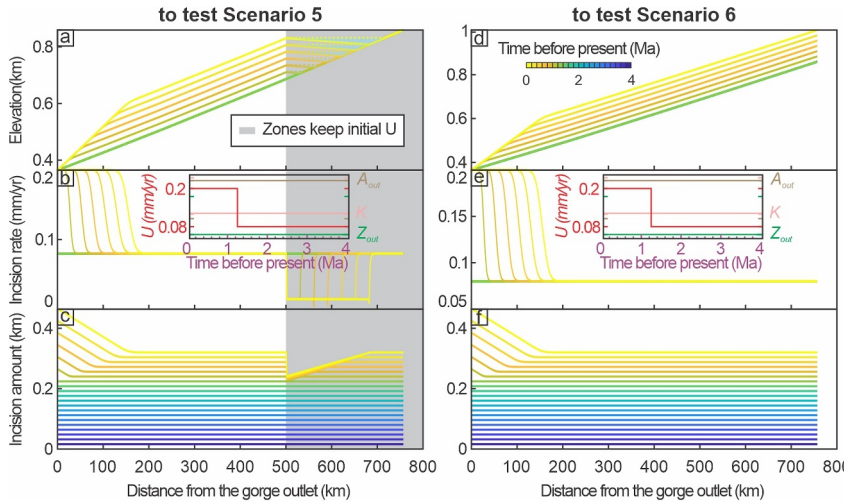

Figure 4. Changes in simulated channel profiles, incision rate and amount from 4 Ma to present with suddenly increased uplift rate from 0.08 mm/yr to 0.2 mm/yr since 1.2 Ma, but the variations are applied either within 500 km (a–c) upstream from the gorge outlet or along the whole gorge (d–f). Upstream drainage area, outlet elevation and K are constant through time. Gray bars mark areas where new uplift rates are applied.

applied an uncertainty analysis for testing scenario 2 with different K values, taken from Zhong et al. (2024), and did not find significant changes (Figure S2 in Supporting Information S1).

4.2. Simulated Evolution With Perturbations in Outlet Elevation and Drainage Area Occurring at 0.25 Ma (Scenario 3)

We illustrate that the simulation for this scenario was equivalent to that of scenario 2 (Section 4.1), except that the inflection had less time to propagate upstream and the profile had less time to adjust to the change in upstream drainage area (Figures 3d–3f). Here, the inflection retreated ~50 km from the gorge outlet, compared to ~200 km in scenario 2 (Figures 3a–3c).

4.3. Simulated Evolution With Variations in Uplift Rates in Space and Time Since 1.2 Ma (Scenario 4–12)

In this section, we describe results from scenarios involving accelerated uplift rates. These scenarios include those limiting accelerated uplift to the first 100 or 500 km upstream of the gorge outlet (scenarios 4, 5, 7–11), one with accelerated uplift along the whole gorge (scenario 6), and one in which uplift rates decrease linearly upstream from the gorge outlet (scenario 12).

4.3.1. With Accelerated Uplift Limited to the First 100 km or 500 km Upstream of the Gorge Outlet

We set uplift rate to increase from 0.08 mm/yr starting at 1.2 Ma along the whole gorge either suddenly (Figures 3g–3i, 4a–4c, and S5 in Supporting Information S1), linearly (Figures S3 and S6 in Supporting Information S1), or stepwise (Figures S4 and S7 in Supporting Information S1) to 0.2 mm/yr. We apply this increase in uplift rates only within the first 100 km or 500 km upstream of the gorge outlet. In each case, a decrease in incision rates occurred at the spatial break in uplift rates and retreated upstream. Incision rates in other parts of the gorge increased or remained relatively stable through time (Figures 3g–3i, 4a–4c, and S3–S7 in Supporting Information S1). Such spatial heterogeneity produced a low gradient section along the channel profile at the spatial break, which would likely result in the formation of a lake (marked in transparent blue in Figures 3g–3i, 4a–4c, and S3–S7 in Supporting Information S1). If such a lake did emerge, the erosive power of the channels downstream the spatial break in uplift rates would significantly decrease. We accounted for this effect by decreasing the upstream drainage area for the whole section downstream of the uplift break. We model scenarios including (Figures 3g–3i, 4a–4c, S3 and S4 in Supporting Information S1) or not including (Figures S5–S7 in Supporting Information S1) upstream drainage area above the spatial break in uplift rates, and find steeper channel profiles downstream of the lake when the upstream drainage area was reduced (Figures S5–S7 in Supporting Information S1). We conducted two uncertainty analysis for testing scenario 4, one with different K values (Figure S8 in Supporting

19449194, 2025, 5, Downloaded from https://agupubs.onlinelibrary.wiley.com/doi/10.1029/2024TC008501 by Helmholtz-Zentrum Potsdam GFZ, Wiley Online Library on [19/06/2025]. See the Terms and Conditions (https://onlinelibrary.wiley.com/terms-and-conditions) on Wiley Online Library for rules of use; OA articles are governed by the applicable Creative Commons License

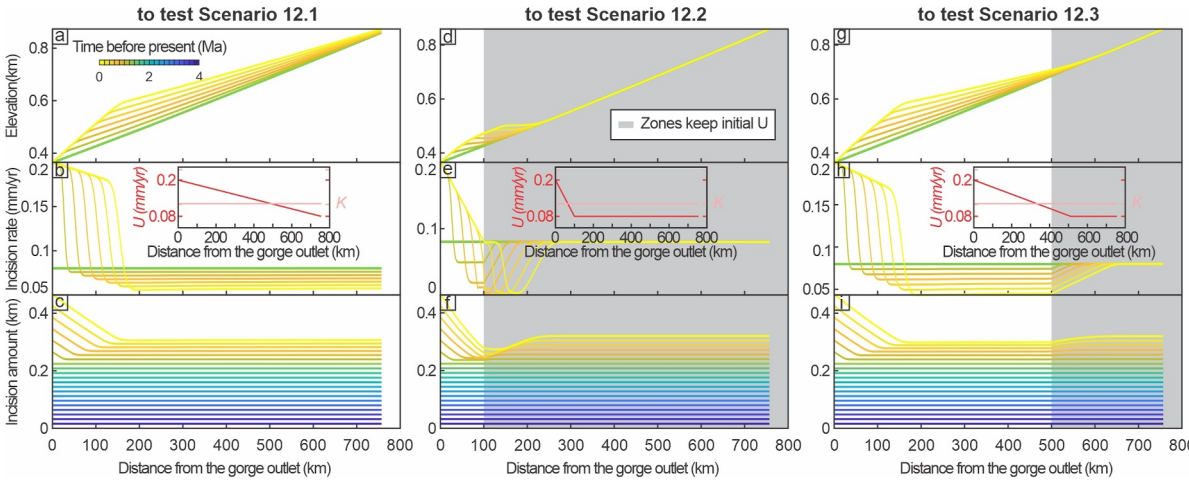

Figure 5. Changes in simulated channel profiles, incision rate and amount from 4 Ma to present with spatially linear reduce from 0.2 mm/yr to 0.08 mm/yr since 1.2 Ma, and the variations are only applied along the whole gorge (a–c), or only within 100 km upstream from gorge outlet (d–f), or only within 500 km upstream from gorge outlet (g–i).

Information S1), and the other with various U values (Figure S9 in Supporting Information S1). These simulated results did not show considerable variations although we changed K or U (Figures S8 and S9 in Supporting Information S1).

4.3.2. With Accelerate Uplift Along the Whole Gorge

In scenario 6, we impose accelerated uplift rate to the whole gorge, that is, without a spatial break in uplift rate along the gorge. An inflection that separates steeper downstream and gentler upstream portions of the gorge emerged after the perturbation at 1.2 Ma. The gentler upstream part maintained the same slope as the initial steady state prior to the 1.2 Ma perturbation (Figure 4d). The inflection migrated progressively upstream, and reached nearly 200 km from the gorge outlet by the present. Once the inflection has passed a given point, the incision rate at that point increased to 0.2 mm/yr, equal to the new uplift rate (Figure 4e). The total amount of incision was highest at the gorge outlet, and gradually decreased upstream following the inflection retreat (Figure 4f).

4.3.3. Linear Reduction in Uplift Rate From the Gorge's Outlet to Its Inlet

Since the sharp spatial break in uplift rate (scenarios 4, 5, 7–11) induced a lake within the gorge, we also explore the impact on channel profiles and incision rates of a gentler gradient in uplift along the gorge. We applied a linear decrease from 0.2 mm/yr to 0.08 mm/yr starting at 1.2 Ma either along the whole gorge (Figure 5b), within the first 100 km upstream from gorge outlet (Figure 5e), or within the first 500 km upstream from gorge outlet (Figure 5h). With these gentler spatial gradients in uplift rate, no lake formed (Figures 5a, 5d, and 5g).

4.4. Simulated Evolution With Variations in K That Vary With Temporal Climate Change (Scenario 13)

As K varied through time, channel profiles developed an inflection that separated steeper downstream and gentler upstream, reflecting a general decrease in K over the modeled time frame (Figure 6a). Incision rates fluctuated, especially at the downstream end of the gorge, while at the upstream end, incision rates showed less spatial variability, and broadly decreased over time (Figure 6b). The total incision amount gradually decreased upstream, with the highest value at the gorge outlet (Figure 6c).

5. Discussion

5.1. Comparison With Incision History From River Terraces and Tributary Channel Profile Analysis

To assess the likelihood of each of the different scenarios, we compare our simulated results with the incision history inferred from river terraces and tributary channel profile analysis.

19449194, 2025, 5, Downloaded from https://agupubs.onlinelibrary.wiley.com/doi/10.1029/2024TC008501 by Helmholtz-Zentrum Potsdam GFZ, Wiley Online Library on [19/06/2025]. See the Terms and Conditions (https://onlinelibrary.wiley.com/terms-and-conditions) on Wiley Online Library for rules of use; OA articles are governed by the applicable Creative Commons License

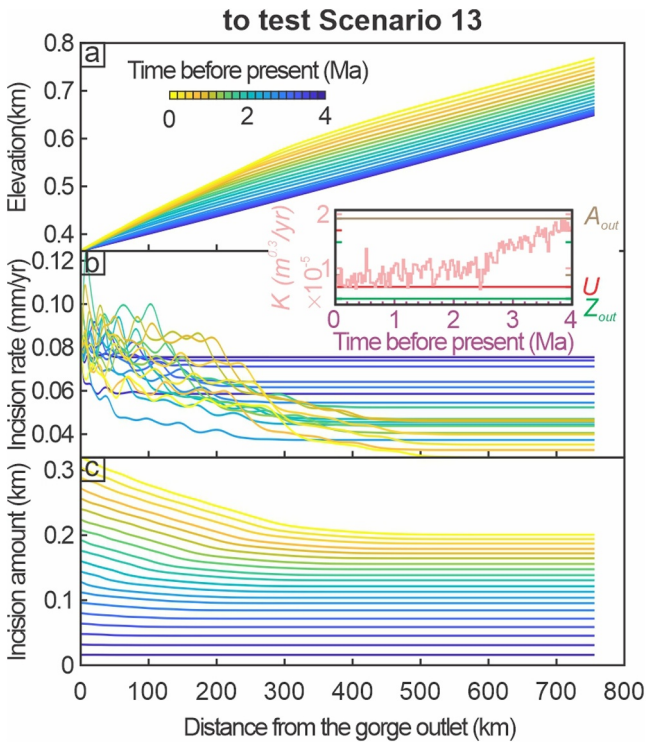

Figure 6. Changes in simulated channel profiles (a), incision rate (b) and amount (c) from 4 Ma to present with temporally changed K values. Upstream drainage area, outlet elevation and uplift rate are constant through time.

Scenarios 2 and 3 only generated a short-lived pulse in incision rates (Figures 3b and 3e), which was inconsistent with the observed long-term (in the past ~1 Ma) increase in incision rate (Figure 2c). Furthermore, simulated slopes of the channel profile were similar upstream and downstream of the inflection (Figures 3a and 3d), while the modern Yellow River profile along the Jinshan Gorge is steeper downstream (i.e., within ~200 km upstream from the gorge outlet) than upstream (Figure 2c).

Scenarios with accelerated uplift rates (scenarios 4–12) showed steeper downstream channel profiles than upstream, which was consistent with the observed modern channel profiles (Figure 2c). In addition, these scenarios also recreated a long-term increase in incision rate and higher incision amount, consistent with the incision history inferred from tributary channel profile analysis and/or river terraces (Figure 2). However, scenarios with a spatial break (scenarios 4, 5, 7–11) or linear reduction (scenario 12) in uplift rate also included a temporal decrease in incision rate upstream, significant either in spatial extent or in magnitude, which was not recorded by tributary channel profile analysis (Figure 2c). We find that scenario 6 did not show such a temporal decrease in incision rate, which therefore suggests that this scenario can best explain the main features recorded by river terraces and inferred from inversion analysis of tributary profiles.

On the one hand, Scenario 13 also resulted it steeper downstream channel profiles (Figure 6a) and higher amounts of incision in the downstream part of the gorge (Figure 6c), consistent with observations. On the other hand, it included a general long-term decrease in incision rate (Figure 6b) that was inconsistent with inferences from river terraces and inversion analysis of tributary profiles. However, it should also be noted that higher amplitude fluctuations in climate on glacial-interglacial time scales in the Pleistocene (Figure S1 in Supporting Information S1) likely lead to higher erosion and sediment transport efficiency. It is difficult to incorporate this aspect of the fluvial response to climate change within the framework of the stream power law we apply here, which could lead to discrepancies between our simulation in Figure 6b and actual incision rate variations on glacial-interglacial time scales in the Pleistocene.

5.2. Inverse Analysis of Channel Profiles Along the Jinshan Gorge

We find that simulated incision variations in space and time following perturbations to uplift rates at 1.2 Ma with a large-scale spatial break or even gentler spatial variations in uplift rates were not consistent with incision variations observed from river terraces and tributary profile inversion analysis. Rather, a relatively uniform increase in uplift rates along the whole gorge (scenario 6) better recreated the observables.

The inversion results (Figure 7) showed that uplift rates, relative to the Weihe Graben, which serves as the local base level (Figure 1), and incision rates along the Jinshan Gorge were generally low (~0.04 mm/yr) and steady prior to the Early Pliocene, which was consistent with previous inferences that the Ordos Block was tectonically stable (L. Xiong & Tang, 2019). The inversion suggested that rates then continuously increased to ~0.16 mm/yr since the Early Pliocene, with an acceleration since the Pleistocene (Figure 7). We omitted Channels in the deserts on the Ordos Block, dominated by aeolian processes (Kapp et al., 2015), and to the east of the Jinshan Gorge that might be influenced by the uplift of the Lvliang Mountain (Figure 1b) here. We also performed a second inversion with no channels omitted. Results of this inversion are shown in the supplement (Figure S11 in Supporting Information S1); no significant difference is found.

5.3. Possible Reasons for the Accelerated Uplift and Incision Rates Since the Early Pliocene

Variations in river incision rates are commonly attributed to either internal drainage basin reorganization (e.g., Fan et al., 2018; Rohrmann et al., 2023; Willett et al., 2014) or external perturbations in climate and tectonics (e.g., Burbank & Anderson, 2011; Molnar & England, 1990; Pan et al., 2009; Wegmann & Pazzaglia, 2002). As tributary basins along the Jinshan Gorge are thought to have experienced little network reorganization (Willett

19449194, 2025, 5, Downloaded from https://agupubs.onlinelibrary.wiley.com/doi/10.1029/2024TC008501 by Helmholtz-Zentrum Potsdam GFZ, Wiley Online Library on [19/06/2025]. See the Terms and Conditions (https://onlinelibrary.wiley.com/terms-and-conditions) on Wiley Online Library for rules of use; OA articles are governed by the applicable Creative Commons License

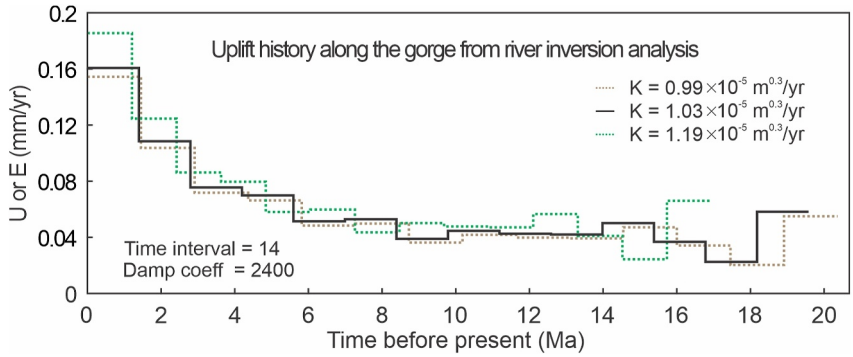

Figure 7. Inferred uplift history relative to the Weihe Graben or incision history for channels along the Jinshan Gorge. Absolute rate and time obtained with $K = 1.03 \times 10^{-5}$ $m^{0.3}$/yr. Uncertainty ranges estimated with $K = 1.19$ or 0.99×10^{-5} $m^{0.3}$/yr.

et al., 2014) and large-scale river integration is not likely to have occurred in the middle Yellow River (Section 5.1), our inferred increase in river incision rates since the Early Pliocene is likely related to external perturbations.

Climate change on million-year timescales in the Ordos Block is characterized by a sustained aridity and cooling with intense oscillations since the Late Pliocene, whereas between the Late Miocene to the Early Pliocene the environment was warm and humid with weaker oscillation (An et al., 2001; Ding et al., 2005; Song et al., 2007, 2014; J. Xiong et al., 2018). In our simulations, temporal climate change resulted in reduced river incision rates (Figure 6b). Nevertheless, river terraces studies along the Jinshan Gorge indicate either constant or increasing incision rates starting from 1.2 Ma (Hu et al., 2016; Liang, 2017; Zhong et al., 2022). It has been reported that erosion can increase when precipitation rates decrease due to a reduction in vegetation protecting alluvial sediment in river valleys (Hall, 1990). However, in our study area, streams mostly incise bedrock, rather than alluvial sediment (Zhong et al., 2024). It has also been suggested that, under a cooling climate, accelerated mountain erosion occurred worldwide, mainly driven by glacial erosion (Herman et al., 2013; Molnar & England, 1990). However, elevations of river networks on the Loess Plateau are mostly below 2,000 m (Figures 1b and S10 in Supporting Information S1), so we do not expect glacial erosion occurred locally.

Spatial variations in climate along the Jinshan Gorge may also influence incision. Annual precipitation rates near the gorge's outlet are ~43% higher than at its upstream end (Figure S10 in Supporting Information S1). As incision rate is ultimately decided by uplift rate, spatial variations in precipitation rates will influence the slope of channel profiles. If no significant spatial or temporal variation in uplift exists along the Jinshan Gorge, modeled channel profiles near the gorge outlet would be gentler, due to its higher precipitation, than modeled channel profiles that use drainage area alone as a proxy for discharge. Including this kind of climate impact on the channel profile would require uplift since the Early Pliocene to increase more than in the inversion results shown in Figure 7. However, we do not expect the difference to be significant, since no northward decreasing trend in the best-fit K values for the lower, middle and upper Jinshan Gorge are found (Zhong et al., 2022). We therefore suggest that temporal and spatial variations in climate is probably not the factor controlling variations in incision rate in the middle Yellow River.

If only the southern Ordos Block is uplifting, that is, if differential uplift exists between the northern and southern parts of the Block, we should observe a decrease in incision somewhere along the trunk channel of the Jinshan Gorge. As the southern part serves as a local base-level for the northern part, if the southern part uplifts faster, the northern part would experience base-level rise, which would result in decreased incision rates there (Figures 3g–3i, 4a–4c, 5 and S3–S9 in Supporting Information S1). However, incision rates in the northern part are mostly steady or even slightly increasing through time, as inferred from river terraces and channel profiles (Figure 2). We therefore do not believe the southern Ordos Block has uplifted independently from the northern part, and propose a modified version of the interpretation of Zhong et al. (2022).

The spatial and temporal pattern of incision rate along the Jinshan Gorge is more consistent with a fall in base level driven by surface lowering in the Weihe Graben (Figures 4d–4f), rather than uplift of only the southern

19449194, 2025, 5, Downloaded from https://agupubs.onlinelibrary.wiley.com/doi/10.1029/2024TC008501 by Helmholtz-Zentrum Potsdam GFZ, Wiley Online Library on [19/06/2025]. See the Terms and Conditions (https://onlinelibrary.wiley.com/terms-and-conditions) on Wiley Online Library for rules of use; OA articles are governed by the applicable Creative Commons License

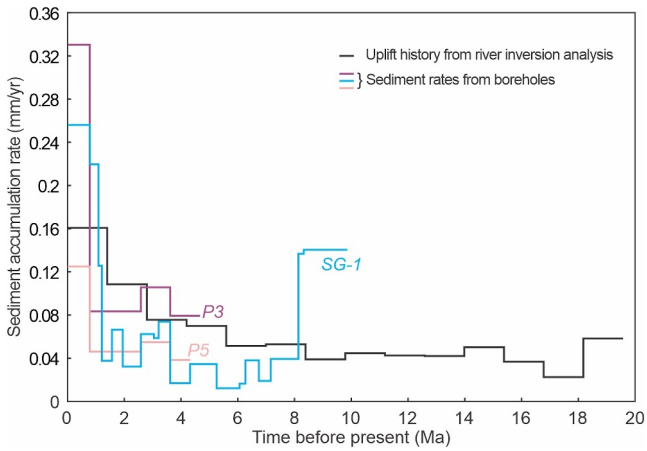

Figure 8. Sediment rates from boreholes SG-1, P3 and P5. The figure is modified from (Yan et al., 2020). The inferred relative uplift or incision rate function with channels in the deserts and to the east of the Jinshan Gorge remove shown in red dashed line.

Ordos Block (Figures 3g–3i, 4a–4c, 5 and S3–S9 in Supporting Information S1). Surface lowering in the Weihe Graben could be obtained if an acceleration in subsidence is not compensated by increased sedimentation. In this scenario, the history of uplift and incision we obtained is relative to the remainder of the subsidence rate in the Weihe Graben minus its sedimentation rate.

5.4. Evidence for Accelerated Subsidence of the Weihe Graben From Other Observations

Geophysical exploration in the Weihe Graben shows that the thickness of Cenozoic deposits ranges from 2 to 7 km, thinning toward the north (Sun, 2005). The maximum thickness of Quaternary sedimentation reaches 1.2 km, associated with the largest average sedimentation rate of 0.47 mm/yr, while a lower rate of ∼0.08 mm/yr is found during the Paleogene and Neogene (Sun, 2005). Better constraints on variations of sedimentation rate near the fault bounding the outlet of the Jinshan Gorge are given by borehole data (Figure 1b). Since the Pliocene, sedimentation rates in boreholes SG-1 (Yan et al., 2020), P3 and P5 (Q. Wang et al., 2002) continuously increased, with significant acceleration since the Middle Pleistocene (Yan et al., 2020) (Figure 8). It is noted that sedimentation rates since 155 AD on a shorter ($\leq 10^3$ a) timescale show much higher values (Xu, 2013), which may have been a result of anthropogenic fluctuations in sediment supply (Ren, 2015). A possible alternative interpretation could be that the accelerated sediment accumulation in the Weihe Graben is related to the globally observed increase in sedimentation rates since ∼2–4 Ma in response to increased erosion rates associated with climate cooling (P. Zhang et al., 2001). However, if the acceleration in sedimentation rate was not accommodated by analogous subsidence of the Weihe Graben, then the Yellow River would incise into its deposits and form a gorge, which is not the case in the modern Weihe Graben (Figure 1b).

Paleoseismic studies on the main normal faults bounding the Weihe Graben yielded vertical slip rates in the range 1–3 mm/yr since the Late Pleistocene (Y. Cheng et al., 2018; Lin et al., 2015; Rao et al., 2014, 2015, 2017), and the slip rate of the southern normal fault bounding the Graben is estimated to be 0.25 mm/yr over the last 3 Ma (J. Xiong et al., 2018). Both of these values are larger than the inferred incision rates along the Jinshan Gorge (Figure 7). Combining incision rates along the Jinshan Gorge and sedimentation rates in the Weihe Graben (Figures 7 and 8) yields a total average rate of 0.2–0.3 mm/yr in the last 3 Ma, which is consistent with the slip rate of the southern normal fault bounding the graben (J. Xiong et al., 2018). A total average rate in the past ∼1 Ma is generally smaller than 0.5 mm/yr (Figures 7 and 8), which is less than half of boundary fault slip rate since the Late Pleistocene (Y. Cheng et al., 2018; Lin et al., 2015; Rao et al., 2014, 2015, 2017). However, the larger difference could be due to a Sadler effect as the observations are made on different timescales (Sadler, 1981). Collectively, slip rates of the faults bounding the Weihe Graben from paleoseismic studies are large enough and their variations are likely sufficient to account for the observed changes in incision rates along the gorge and sedimentation rates in the graben.

The inferred Pliocene to Pleistocene increase of slip rate of the main normal faults bounding the Weihe Graben could be due to focusing of deformation and fault integration on the main boundary faults (Shi et al., 2015, 2019, 2020; Y. Zhang et al., 2003). Studies of the tectonic evolution of structures fringing the Ordos Block from fault kinematic analysis showed that the eastern and northern marginal grabens formed as pull-apart basins in response to a transtensional stress regime since the Late Miocene (Shi et al., 2020). From the Late Miocene to the Early Pleistocene, the stress field showed a NW-SE extensional and NE-SW compressional regime around the Ordos Block (Shi et al., 2019). During this period, the crust of the Block's eastern margin deformed and a series of left-stepping en échelon pull-apart basins were formed, due to a NE-trending right-lateral shear stress regime (Y. Zhang et al., 2003). A gentle NE-SW extension in the Late Pleistocene subsequently dominated around the Ordos Block and widespread normal fault activity occurred in the western grabens (Shi et al., 2015). Since the end of the Late Pleistocene, the tectonic regime changed to ENE-WSW compression (China Earthquake Administration, 1988), reactivating preexisting NNE- and ENE-striking faults bounding the Ordos Block (Shi et al., 2020).

19449194, 2025, 5, Downloaded from https://agupubs.onlinelibrary.wiley.com/doi/10.1029/2024TC008501 by Helmholtz-Zentrum Potsdam GFZ, Wiley Online Library on [19/06/2025]. See the Terms and Conditions (https://onlinelibrary.wiley.com/terms-and-conditions) on Wiley Online Library for rules of use; OA articles are governed by the applicable Creative Commons License

19449194, 2025, 5, Downloaded from https://agupubs.onlinelibrary.wiley.com/doi/10.1029/2024TC008501 by Helmholtz-Zentrum Potsdam GFZ, Wiley Online Library on [19/06/2025]. See the Terms and Conditions (https://onlinelibrary.wiley.com/terms-and-conditions) on Wiley Online Library for rules of use; OA articles are governed by the applicable Creative Commons License

5.5. Potential Applicability of Channel Profile Simulations to Other Tectonic Settings for Deciphering Tectonic Histories

Trunk channels flowing long distances may travel across different tectonic settings, that is, considerable spatial changes in uplift rate could exist. A direct application of channel profile inversion analysis without consideration of possible spatial variations in uplift rate likely challenge the reliability of inversion analysis results. In this study we modeled trunk channel profile development from various spatial variations in uplift rate, and compared the results with incision history inferred from tributary profiles, together with profile and river terraces of trunk channel. We provide this as a way to test whether significant spatial differences in uplift rate exist. As channel profiles are ubiquitous along rivers, we suggest channel profile simulations as a powerful tool to decipher tectonic histories in other places, although their tectonic settings are various.

6. Conclusion

Pleistocene increased incision rates of the Yellow River along the Jinshan Gorge have been attributed to paleolake regression in the downstream Weihe Graben and the upstream Hetao Graben, while the influence of local tectonic variations on river incision has been, until now, neglected. In this paper, we have used channel profile simulations of the trunk channel along the Jinshan Gorge to explore explicitly various alternative explanations for variations in the incision pattern. We find that modeled profile development from paleolake regression in the Weihe Graben (which would have driven sudden base level fall in the Jinshan Gorge) or integration with the Hetao Graben (which would have driven an increase in drainage area in the Jinshan Gorge) were not consistent with either the observed modern channel profile of the Jinshan Gorge, or the incision history recorded by river terraces and inferred from an inversion analysis of tributary profiles. Instead, simulated profile evolutions and variations in incision rate due to a recent acceleration of tectonic activity, via topographic lowering in the Weihe Graben, rather than uplift only of the southern Ordos Block, can explain the main features of incision history recorded by terraces and channel profiles. The latter indicates that before the Early Pliocene uplift rates were steady at ∼0.04 mm/yr, then gradually increased to ∼0.16 mm/yr from the Middle Pleistocene until present. The accelerated surface lowering at the Weihe Graben suggested by our channel profile simulations is consistent with other observables, such as variations of sediment accumulation rates from drill cores, changes in boundary fault slip rates from paleoseismic studies, and stress regime variations, collectively suggesting that channel profile simulations can be an efficient way to infer tectonic variations.

Conflict of Interest

The authors declare no conflicts of interest relevant to this study.

Data Availability Statement

The river terrace data (Figure 2a and Table S1 in Supporting Information S1) are available from Cao (2012), Guo et al. (2012), Hu et al. (2016), Z. Li et al. (2020, 2021), Liang (2017), Y. Liu (2014, 2020), Y. Liu et al. (2007), Pan et al. (2012), J. Wang (2006), J. F. Zhang et al. (2011). Borehole data (Figure 8) are available from Q. Wang et al. (2002), Yan et al. (2020). Deep-sea benthic foraminiferal oxygen isotope data from DSDP and ODP (Figure S1a in Supporting Information S1) are available from Zachos et al. (2001). >19 μm grain-size fraction data (Figure S1b in Supporting Information S1) are available from An et al. (2001). The hydrologically conditioned version of the digital elevation model is available through the HydroSHEDS database (Lehner et al., 2008). Annual mean precipitation data are available from WorldClim (Fick & Hijmans, 2017). Channel profiles, incision rate and incision simulations (Figures 3–6 and S2–S9 in Supporting Information S1) were performed on TopoToolbox, a MATLAB-based software (Schwanghart & Scherler, 2014).

Acknowledgments
Sean D. Willett and Eric Kirby are thanked for discussions. Fergus McNab is especially thanked for detailed language corrections. This work was jointly supported by the National Natural Science Foundation of China (Grant 42225205, 42488201), an SNF Postdoc Mobility Fellowship (P500PN_214178), Section 4.6: Geomorphology funding from GFZ.

References

An, Z., Kutzbatch, J. E., Prell, W. L., & Porder, S. C. (2001). Evolution of Asian monsoons and phased uplift of the Himalaya-Tibetan plateau since Late Miocene times [Dataset]. *Nature*, *411*(6833), 62–66. https://doi.org/10.1038/35075035

Burbank, D. W., & Anderson, R. S. (2011). *Tectonic geomorphology*. John Wiley & Sons.

Cao, X. (2012). Low-level river terraces and loess deposits of typical profile from Heiyukou to Zhangjiawan in the middle reach of the Yellow River [Dataset]. *Master Thesis of Southwest University*. https://doi.org/10.7666/d.y2086393

Chen, L., Cheng, C., & Wei, Z. (2009). Seismic evidence for significant lateral variations in lithospheric thickness beneath the central and western North China Craton. *Earth and Planetary Science Letters*, *286*(1–2), 171–183. https://doi.org/10.1016/j.epsl.2009.06.022

Cheng, S., Deng, Q., Zhou, S., & Yang, G. (2002). Strath terraces of Jinshaan Canyon, Yellow River, and quaternary tectonic movements of the Ordos plateau, north China. *Terra Nova*, *14*(4), 215–224. https://doi.org/10.1046/j.1365-3121.2002.00350.x

Cheng, Y., He, C., Rao, G., Yan, B., Lin, A., Hu, J., et al. (2018). Geomorphological and structural characterization of the southern Weihe Graben, central China: Implications for fault segmentation. *Tectonophysics*, *722*(November), 11–24. https://doi.org/10.1016/j.tecto.2017.10.024

China Earthquake Administration. (1988). *Active faults surrounding Ordos plateau*. Seismological Press. (In Chinese).

Clinkscales, C., Kapp, P., Thomson, S., Wang, H., Laskowski, A., Orme, D. A., & Pullen, A. (2021). Regional exhumation and tectonic history of the Shanxi Rift and Taihangshan, north China. *Tectonics*, *40*(3), e2020TC006416. https://doi.org/10.1029/2020tc006416

Craddock, W. H., Kirby, E., Harkins, N. W., Zhang, H., Shi, X., & Liu, J. (2010). Rapid fluvial incision along the Yellow River during headward basin integration. *Nature Geoscience*, *3*(3), 209–213. https://doi.org/10.1038/ngeo777

Crosby, B. T., & Whipple, K. X. (2006). Knickpoint initiation and distribution within fluvial networks: 236 waterfalls in the Waipaoa River, north Island, New Zealand. *Geomorphology*, *82*(1–2), 16–38. https://doi.org/10.1016/j.geomorph.2005.08.023

Ding, Z. L., Derbyshire, E., Yang, S. L., Sun, J. M., & Liu, T. S. (2005). Stepwise expansion of desert environment across northern China in the past 3.5 Ma and implications for monsoon evolution. *Earth and Planetary Science Letters*, *237*(1–2), 45–55. https://doi.org/10.1016/j.epsl.2005.06.036

Fan, N., Chu, Z., Jiang, L., Hassan, M. A., Lamb, M. P., & Liu, X. (2018). Abrupt drainage basin reorganization following a Pleistocene river capture. *Nature Communications*, *9*(1), 3756. https://doi.org/10.1038/s41467-018-06238-6

Fick, S. E., & Hijmans, R. J. (2017). WorldClim 2: New 1-km spatial resolution climate surfaces for global land areas (version 2.1) [Dataset]. *International Journal of Climatology*, *37*(12), 4302–4315. https://doi.org/10.1002/joc.5086

Fox, M., Goren, L., May, D. A., & Willett, S. D. (2014). Inversion of fluvial channels for paleorock uplift rates in Taiwan. *Journal of Geophysical Research: Earth Surface*, *119*(345678), 1853–1875. https://doi.org/10.1002/2014JF003196

Goren, L., Fox, M., & Willett, S. D. (2014). Tectonics from fluvial topography using formal linear inversion: Theory and applications to the Inyo Mountains, California. *Journal of Geophysical Research F: Earth Surface*, *119*(8), 1651–1681. https://doi.org/10.1002/2014JF003079

Guo, Y., Zhang, J., Qiu, W., Hu, G., Zhuang, M., & Zhou, L. (2012). Luminescence dating of the Yellow River terraces in the Hukou area, China [Dataset]. *Quaternary Geochronology*, *10*, 129–135. https://doi.org/10.1016/j.quageo.2012.03.002

Hall, S. A. (1990). Channel trenching and climatic change in the southern U.S. Great Plains. *Geology*, *18*(4), 342–345. https://doi.org/10.1130/0091-7613(1990)018<0342:CTACCI>2.3.CO;2

Herman, F., Seward, D., Valla, P. G., Carter, A., Kohn, B., Willett, S. D., & Ehlers, T. A. (2013). Worldwide acceleration of mountain erosion under a cooling climate. *Nature*, *504*(7480), 423–426. https://doi.org/10.1038/nature12877

Howard, A. D., & Kerby, G. (1983). Channel changes in badlands. *Geological Society of America Bulletin*, *94*(6), 739–752. https://doi.org/10.1130/0016-7606(1983)94<739:ccib>2.0.co;2

Hu, Z., Pan, B., Guo, L., Vandenberghe, J., Liu, X., Wang, J., et al. (2016). Rapid fluvial incision and headward erosion by the Yellow River along the Jinshaan gorge during the past 1.2 Ma as a result of tectonic extension [Dataset]. *Quaternary Science Reviews*, *133*, 1–14. https://doi.org/10.1016/j.quascirev.2015.12.003

Hu, Z., Pan, B. T., Bridgland, D., Vandenberghe, J., Guo, L. Y., Fan, Y. L., & Westaway, R. (2017). The linking of the upper-middle and lower reaches of the Yellow River as a result of fluvial entrenchment. *Quaternary Science Reviews*, *166*, 324–338. https://doi.org/10.1016/j.quascirev.2017.02.026

Jiang, F., Fu, J., Wang, S., Sun, D., & Zhao, Z. (2007). Formation of the Yellow River, inferred from loess-palaeosol sequence in Mangshan and lacustrine sediments in Sanmen Gorge, China. *Quaternary International*, *175*(1), 62–70. https://doi.org/10.1016/j.quaint.2007.03.022

Kapp, P., Pullen, A., Pelletier, J. D., Russell, J., Goodman, P., & Cai, F. (2015). From dust to dust: Quaternary wind erosion of the Mu Us desert and Loess Plateau, China. *Geology*, *43*(9), 835–838. https://doi.org/10.1130/G36724.1

Ke, Z. (2012). Fluvialcompetition: Exemplified by formation and evolution of the Fen River and Jinshan Yellow River. *Quaternary Sciences*, *32*(5), 859–865.

Kong, P., Jia, J., & Zheng, Y. (2014). Time constraints for the Yellow River traversing the Sanmen Gorge. *Geochemistry, Geophysics, Geosystems*, *15*(2), 395–407. https://doi.org/10.1002/2013GC004912

Lehner, B., Verdin, K., & Jarvis, A. (2008). New global hydrography derived from spaceborne elevation data (Version 1.1) [Dataset]. *Eos, Transactions American Geophysical Union*, *89*(10), 93–94. https://doi.org/10.1029/2008eo100001

Li, B., Sun, D., Xu, W., Wang, F., Liang, B., Ma, Z., et al. (2017). Paleomagnetic chronology and paleoenvironmental records from drill cores from the Hetao Basin and their implications for the formation of the Hobq Desert and the Yellow River. *Quaternary Science Reviews*, *156*, 69–89. https://doi.org/10.1016/j.quascirev.2016.11.023

Li, Y., Wang, Q., Cui, D., Hao, M., Ji, L., & Qin, S. (2014). One feature of the activated southern Ordos block: The Ziwuling small earthquake cluster. *Geodesy and Geodynamics*, *5*(3), 16–22. https://doi.org/10.3724/sp.j.1246.2014.03016

Li, Z., Zhang, K., Liang, H., Chen, Z., Li, X., Khan, W., et al. (2020). Initial incision of the Jinshan Gorge of the Yellow River, China, constrained by terrestrial in situ cosmogenic nuclides chronology [Dataset]. *Quaternary International*, *550*(December 2019), 111–119. https://doi.org/10.1016/j.quaint.2020.03.047

Li, Z., Zhang, K., Liang, H., Chen, Z., Ma, Z., Xiong, J., & Huang, P. (2021). Large river chronology along the Jinshaan Gorge on the Yellow River and its implications for initialization [Dataset]. *Geomorphology*, *400*, 108092. https://doi.org/10.1016/j.geomorph.2021.108092

Liang, H. (2017). Long-term fluvial evolution and response to basin connection along the Jinshan-Sanmen Gorge, Yellow River since late mid-Pleistocene [Dataset]. *Ph.D. Thesis of Sun Yat-Sen University*.

Liang, H., Zhang, K., Fu, J., Li, L., Chen, J., Li, S., & Chen, L. (2015). Bedrock river incision response to basin connection along the Jinshan Gorge, Yellow River, north China. *Journal of Asian Earth Sciences*, *114*, 203–211. https://doi.org/10.1016/j.jseaes.2015.07.010

Liang, H., Zhang, K., Li, Z., Fu, J., Yu, Z., Xiong, J., et al. (2022). How headward erosion breaches upstream paleolakes: Insights from dated longitudinal fluvial terrace correlations within the Sanmen Gorge, Yellow River. *GSA Bulletin*. https://doi.org/10.1130/b36537.1

Lin, A., Rao, G., & Yan, B. (2015). Flexural fold structures and active faults in the northern-western Weihe Graben, central China. *Journal of Asian Earth Sciences*, *114*, 226–241. https://doi.org/10.1016/j.jseaes.2015.04.012

Lin, A., Yang, Z., Sun, Z., & Yang, T. (2001). How and when did the Yellow River develop its square bend. *Geology*, *29*(10), 951–954. https://doi.org/10.1130/0091-7613(2001)029<0951:hawdty>2.0.co;2

Liu, J., Zhang, P., Lease, R. O., Zheng, D., Wan, J., Wang, W., & Zhang, H. (2013). Eocene onset and late Miocene acceleration of Cenozoic intracontinental extension in the North Qinling range-Weihe graben: Insights from apatite fission track thermochronology. *Tectonophysics*, *584*, 281–296. https://doi.org/10.1016/j.tecto.2012.01.025

Liu, Y. (2014). Magnetostratigraphy of Red Clay and Silt Layer of Qiujiayan Section, Shenmu County and its implications to the formation of the Yellow River [Dataset]. *Journal of Anqing Teachers College (Natural Science Edition)*, *20*(4), 115–120. https://doi.org/10.13757/j.cnki.cn34-1150/n.2014.04.028

19449194, 2025, 5, Downloaded from https://agupubs.onlinelibrary.wiley.com/doi/10.1029/2024TC008501 by Helmholtz-Zentrum Potsdam GFZ, Wiley Online Library on [19/06/2025]. See the Terms and Conditions (https://onlinelibrary.wiley.com/terms-and-conditions) on Wiley Online Library for rules of use; OA articles are governed by the applicable Creative Commons License

Liu, Y. (2020). Neogene fluvial sediments in the northern Jinshaan Gorge, China: Implications for early development of the Yellow River since 8 Ma and its response to rapid subsidence of the Weihe-Shanxi Graben [Dataset]. *Palaeogeography, Palaeoclimatology, Palaeoecology*, *546*(February), 109675. https://doi.org/10.1016/j.palaeo.2020.109675

Liu, Y., Li, Y., Lu, H., Si, S., & Zhao, H. (2007). Preliminary study of alluvial pebbles on high terraces of the Yellow River from Baode to Kehu in Shanxi-Shaanxi Gorge [Dataset]. *Acta Scientiarum Naturalium Universitatis Pekinensis*, *43*(6), 808–815. Retrieved from https://xbna.pku.edu.cn/EN/Y2007/V43/I6/808

Molnar, P., & England, P. (1990). Late Cenozoic uplift of mountain ranges and global climate change: Chicken or egg? *Nature*, *346*(6279), 29–34. https://doi.org/10.1038/346029a0

Pan, B., Hu, Z., Wang, J., Vandenberghe, J., & Hu, X. (2011). A magnetostratigraphic record of landscape development in the eastern Ordos Plateau, China: Transition from late Miocene and early Pliocene stacked sedimentation to late Pliocene and quaternary uplift and incision by the Yellow River. *Geomorphology*, *125*(1), 225–238. https://doi.org/10.1016/j.geomorph.2010.09.019

Pan, B., Hu, Z., Wang, J., Vandenberghe, J., Hu, X., Wen, Y., et al. (2012). The approximate age of the planation surface and the incision of the Yellow River [Dataset]. *Palaeogeography, Palaeoclimatology, Palaeoecology*, *356–357*, 54–61. https://doi.org/10.1016/j.palaeo.2010.04.011

Pan, B., Su, H., Hu, Z., Hu, X., Gao, H., Li, J., & Kirby, E. (2009). Evaluating the role of climate and tectonics during non-steady incision of the Yellow River: Evidence from a 1.24 Ma terrace record near Lanzhou, China. *Quaternary Science Reviews*, *28*(27–28), 3281–3290. https://doi.org/10.1016/j.quascirev.2009.09.003

Perrineau, A., Woerd, J. V. D., Gaudemer, Y., Liu-Zeng, J., Pik, R., Tapponnier, P., et al. (2011). Incision rate of the Yellow River in northeastern Tibet constrained by ^{10}Be and ^{26}Al cosmogenic isotope dating of fluvial terraces: Implications for catchment evolution and plateau building. *Geological Society, London, Special Publications*, *353*(1), 189–219. https://doi.org/10.1144/SP353.10

Rao, G., Cheng, Y., Yu, Y., Yan, B., & Lin, A. (2017). Tectonic characteristics of the Lishan Piedmont fault in the SE Weihe Graben (central China), as revealed by the geomorphological and structural analyses. *Geomorphology*, *282*, 52–63. https://doi.org/10.1016/j.geomorph.2017.01.014

Rao, G., Lin, A., & Yan, B. (2015). Paleoseismic study on active normal faults in the southeastern Weihe Graben, central China. *Journal of Asian Earth Sciences*, *114*, 212–225. https://doi.org/10.1016/j.jseaes.2015.04.031

Rao, G., Lin, A., Yan, B., Jia, D., & Wu, X. (2014). Tectonic activity and structural features of active intracontinental normal faults in the Weihe Graben, central China. *Tectonophysics*, *636*, 270–285. https://doi.org/10.1016/j.tecto.2014.08.019

Ren, M. (2015). Sediment discharge of the Yellow River, China: Past, present and future—A synthesis. *Acta Oceanologica Sinica*, *34*(2), 1–8. https://doi.org/10.1007/s13131-015-0619-6

Ritts, B. D., Weislogel, A., Graham, S. A., & Darby, B. J. (2009). Mesozoic tectonics and sedimentation of the giant polyphase nonmarine intraplate Ordos Basin, Western North China Block. *International Geology Review*, *51*(2), 95–115. https://doi.org/10.1080/00206810802614523

Roberts, G. G., Paul, J. D., White, N., & Winterbourne, J. (2012). Temporal and spatial evolution of dynamic support from river profiles: A framework for Madagascar. *Geochemistry, Geophysics, Geosystems*, *13*(4), 1–23. https://doi.org/10.1029/2012GC004040

Roberts, G. G., & White, N. (2010). Estimating uplift rate histories from river profiles using African examples. *Journal of Geophysical Research*, *115*(2), 1–24. https://doi.org/10.1029/2009JB006692

Rohrmann, A., Kirby, E., & Schwanghart, W. (2023). Accelerated Miocene incision along the Yangtze River driven by headward drainage basin expansion. *Science Advances*, *9*(36), eadh1636. https://doi.org/10.1126/sciadv.adh1636

Sadler, P. M. (1981). Sediment accumulation rates and the completeness of stratigraphic sections. *The Journal of Geology*, *89*(5), 569–584. https://doi.org/10.1086/628623

Schwanghart, W., & Scherler, D. (2014). TopoToolbox 2–MATLAB-based software for topographic analysis and modeling in Earth surface sciences (Version 2.4) [Software]. *Earth Surface Dynamics*, *2*(1), 1–7. https://doi.org/10.5194/esurf-2-1-2014

Shi, W., Chen, L., Chen, X., Cen, M., & Zhang, Y. (2019). The Cenozoic tectonic evolution of the faulted basins in the northern margin of the Eastern Qinling Mountains, Central China: Constraints from fault kinematic analysis. *Journal of Asian Earth Sciences*, *173*, 204–224. https://doi.org/10.1016/j.jseaes.2019.01.018

Shi, W., Dong, S., & Hu, J. (2020). Neotectonics around the Ordos Block, north China: A review and new insights. *Earth-Science Reviews*, *200*(September 2019), 102969. https://doi.org/10.1016/j.earscirev.2019.102969

Shi, W., Dong, S., Liu, Y., Hu, J., Chen, X., & Chen, P. (2015). Cenozoic tectonic evolution of the south ningxia region, northeastern Tibetan plateau inferred from new structural investigations and fault kinematic analyses. *Tectonophysics*, *649*, 139–164. https://doi.org/10.1016/j.tecto.2015.02.024

Song, Y., Fang, X., King, J. W., Li, J., Naoto, I., & An, Z. (2014). Magnetic parameter variations in the Chaona loess/paleosol sequences in the central Chinese Loess Plateau, and their significance for the middle Pleistocene climate transition. *Quaternary Research*, *81*(3), 433–444. https://doi.org/10.1016/j.yqres.2013.10.002

Song, Y., Fang, X., Torii, M., Ishikawa, N., Li, J., & An, Z. (2007). Late Neogene rock magnetic record of climatic variation from Chinese eolian sediments related to uplift of the Tibetan Plateau. *Journal of Asian Earth Sciences*, *30*(2), 324–332. https://doi.org/10.1016/j.jseaes.2006.10.004

Sun, J. (2005). Long-term fluvial archives in the Fen Wei Graben, central China, and their bearing on the tectonic history of the India-Asia collision system during the Quaternary. *Quaternary Science Reviews*, *24*(10–11), 1279–1286. https://doi.org/10.1016/j.quascirev.2004.08.018

Tapponnier, P., & Molnar, P. (1976). Slip-line field theory and large-scale continental tectonics. *Nature*, *264*(5584), 319–324. https://doi.org/10.1038/264319a0

Wang, J. (2006). Formation and evolution of the middle reaches of the Yellow River since late Cenozoic [Dataset]. *Ph.D. Thesis of Lanzhou University*. https://doi.org/10.7666/d.Y917959

Wang, Q., Li, C., Tian, G., Zhang, W., Liu, C., Ning, L., et al. (2002). Tremendous change of the earth surface system and tectonic setting of salt-lake formation in Yuncheng Basin since 7.1 Ma [Dataset]. *Science in China - Series D: Earth Sciences*, *45*(2), 110–122. https://doi.org/10.1007/bf02879788

Wegmann, K. W., & Pazzaglia, F. J. (2002). Holocene strath terraces, climate change, and active tectonics: The Clearwater River basin, Olympic Peninsula, Washington State. *Bulletin of the Geological Society of America*, *114*(6), 731–744. https://doi.org/10.1130/0016-7606(2002)114<0731:HSTCCA>2.0.CO;2

Whipple, K. X., & Tucker, G. E. (1999). Dynamics of the stream-power river incision model: Implications for height limits of mountain ranges, landscape response timescales, and research needs. *Journal of Geophysical Research*, *104*(B8), 17661–17674. https://doi.org/10.1029/1999JB900120

Willett, S. D., McCoy, S. W., Taylor Perron, J., Goren, L., & Chen, C. Y. (2014). Dynamic reorganization of river basins. *Science*, *343*(6175). https://doi.org/10.1126/science.1248765

19449194, 2025, 5, Downloaded from https://agupubs.onlinelibrary.wiley.com/doi/10.1029/2024TC008501 by Helmholtz-Zentrum Potsdam GFZ, Wiley Online Library on [19/06/2025]. See the Terms and Conditions (https://onlinelibrary.wiley.com/terms-and-conditions) on Wiley Online Library for rules of use; OA articles are governed by the applicable Creative Commons License

Xiao, G., Sun, Y., Yang, J., Yin, Q., Dupont-Nivet, G., Licht, A., et al. (2020). Early Pleistocene integration of the Yellow River I: Detrital-zircon evidence from the North China Plain. *Palaeogeography, Palaeoclimatology, Palaeoecology*, *546*(December 2019), 109691. https://doi.org/10.1016/j.palaeo.2020.109691

Xiong, J., Li, Y., Zheng, W., Zhang, P., Lei, J., Zhong, Y., et al. (2018). Climatically driven formation of the Tangxian planation surface in north China: An example from northwestern Zhongtiao Shan of the Shanxi Graben System. *Lithosphere*, *10*(4), 530–544. https://doi.org/10.1130/L720.1

Xiong, J., Zhang, P., Deng, C., Picotti, V., Liang, H., Ren, Z., et al. (2024). Neogene–Quaternary channel evolution and provenance shift of the middle Yellow River. *Journal of Geophysical Research: Earth Surface*, *129*(10), e2023JF007532. https://doi.org/10.1029/2023jf007532

Xiong, L., & Tang, G. (2019). *Loess Landform inheritance: Modeling and discovery*. Springer.

Xu, J. (2013). Sediment storage in the reach of the middle Yellow River located in the Fenwei Graben, China. *Hydrological Processes*, *27*(18), 2623–2636. https://doi.org/10.1002/hyp.9401

Yan, J., Hu, J., Gong, W., Liu, X., Yin, Y., & Tan, C. (2020). Late Cenozoic magnetostratigraphy of the Yuncheng Basin, central north China Craton and its tectonic implications [Dataset]. *Geological Journal*, *55*(11), 7415–7428. https://doi.org/10.1002/gj.3744

Zachos, J., Pagani, H., Sloan, L., Thomas, E., & Billups, K. (2001). Trends, rhythms, and aberrations in global climate 65 Ma to present [Dataset]. *Science*, *292*(5517), 686–693. https://doi.org/10.1126/science.1059412

Zhang, J. F., Wang, X. Q., Qiu, W. L., Shelach, G., Hu, G., Fu, X., et al. (2011). The paleolithic site of Longwangchan in the middle Yellow River, China: Chronology, paleoenvironment and implications [Dataset]. *Journal of Archaeological Science*, *38*(7), 1537–1550. https://doi.org/10.1016/j.jas.2011.02.019

Zhang, P., Molnar, P., & Downs, W. R. (2001). Increased sedimentation rates and grain sizes 2-4 Myr ago due to the influence of climate change on erosion rates. *Nature*, *410*(6831), 891–897. https://doi.org/10.1038/35073504

Zhang, Y., & Liao, C. (2006). Transition of the late Mesozoic–Cenozoic tectonic regimes and modification of the Ordos basin. *Geology in China*, *33*(1), 28–40.

Zhang, Y., Ma, Y., Yang, N., Shi, W., & Dong, S. (2003). Cenozoic extensional stress evolution in North China. *Journal of Geodynamics*, *36*(5), 591–613. https://doi.org/10.1016/j.jog.2003.08.001

Zhang, Y., Mercier, J. L., & Vergély, P. (1998). Extension in the Graben systems around the Ordos (China), and its contribution to the extrusion tectonics of south China with respect to Gobi-Mongolia. *Tectonophysics*, *285*(1–2), 41–75. https://doi.org/10.1016/S0040-1951(97)00170-4

Zheng, H., Huang, X., Ji, J., Liu, R., Zeng, Q., & Jiang, F. (2007). Ultra-high rates of loess sedimentation at Zhengzhou since Stage 7: Implication for the Yellow River erosion of the Sanmen Gorge. *Geomorphology*, *85*(3–4), 131–142. https://doi.org/10.1016/j.geomorph.2006.03.014

Zhong, Y., Picotti, V., Xiong, J., Willett, S. D., Schmidt, C., & King, G. (2024). New data on tributary terraces and a reappraisal of the incision history of the Jinshan Gorge, middle Yellow River. *Geomorphology*, *462*, 109330. https://doi.org/10.1016/j.geomorph.2024.109330

Zhong, Y., Willett, S. D., Picotti, V., Xiong, J., & Zhang, H. (2022). Spatial and temporal variations of incision rate of the middle Yellow River and its tributaries. *Journal of Geophysical Research: Earth Surface*, *127*, 1–15. https://doi.org/10.1029/2021jf006327

19449194, 2025, 5, Downloaded from https://agupubs.onlinelibrary.wiley.com/doi/10.1029/2024TC008501 by Helmholtz-Zentrum Potsdam GFZ, Wiley Online Library on [19/06/2025]. See the Terms and Conditions (https://onlinelibrary.wiley.com/terms-and-conditions) on Wiley Online Library for rules of use; OA articles are governed by the applicable Creative Commons License